J Biol Phys (2013) 39:15–35
DOI 10.1007/s10867-012-9283-7

ORIGINAL PAPER

Nano breathers and molecular dynamics simulations in hydrogen-bonded chains

L. Kavitha · A. Muniyappan · A. Prabhu · S. Zdravković · S. Jayanthi · D. Gopi

Received: 24 June 2012 / Accepted: 13 August 2012 / Published online: 12 October 2012

Abstract Non-linear localization phenomena in biological lattices have attracted a steadily growing interest and their existence has been predicted in a wide range of physical settings. We investigate the non-linear proton dynamics of a hydrogen-bonded chain in a semi-classical limit using the coherent state method combined with a Holstein–Primakoff bosonic representation. We demonstrate that even a weak inherent discreteness in the hydrogen-bonded (HB) chain may drastically modify the dynamics of the non-linear system, leading to instabilities that have no analog in the continuum limit. We suggest a possible localization mechanism of polarization oscillations of protons in a hydrogen-bonded chain through modulational instability analysis. This mechanism arises due to the neighboring proton–proton interaction and coherent tunneling of protons along hydrogen bonds and/or around heavy atoms. We present a detailed analysis of modulational instability, and highlight the role of the interaction strength of neighboring protons in the process of bioenergy localization. We perform molecular dynamics simulations and demonstrate the existence of nanoscale discrete breather (DB) modes in the hydrogen-bonded chain. These highly

L. Kavitha (✉) · A. Muniyappan · A. Prabhu · S. Jayanthi
Department of Physics, Periyar University, Salem 636 011, India
e-mail: louiskavitha@yahoo.co.in

L. Kavitha
The Abdus Salam International Centre for Theoretical Physics, Trieste, Italy

L. Kavitha · D. Gopi
Center for Nanoscience and Nanotechnology, Periyar University, Salem 636 011, Tamilnadu, India

S. Zdravković
Institut za nuklearne nauke Vinča, Univerzitet u Beogradu, Poštanski fah 522, 11001 Beograd, Serbia

D. Gopi
Department of Chemistry, Periyar University, Salem 636 011, India

localized and long-lived non-linear breather modes may play a functional role in targeted energy transfer in biological systems.

Keywords Modulational instability · Hydrogen-bonded chains · Discrete breathers · Solitons · Molecular dynamics simulations · Proton dynamics in biological lattices

1 Introduction

There has recently been substantial interest in the study of collective proton motion in hydrogen-bonded (HB) chains. The transport of energy and charge along one-dimensional HB chains is an extremely important problem in bioenergetic systems, such as bacteriorhodopsin, which pumps protons to higher free energies, and the ATP synthase that consumes energetic protons [1, 2]. In addition, it may be noted that proton transport has been implicated in transhydrogenase [3, 4], cytochrome oxidase, and the bc_1 redox loop in mitochondrial respiratory chains [5, 6]. Indeed, one requires proton transport for long distances along the membrane rather than just proton transport across the membrane. It is also possible to imagine that even more extensive networks of proton pathways exist in the cell, perhaps utilizing the cytosol microstructure [7, 8]. Thus, proton transport may be a part of other bioenergetic mechanisms such as muscle action [9] or flagellar motion [10]. Bioenergy transport through proton dynamics in hydrogen-bonded chains still remains an intriguing phenomenon to most physicists and biologists. A strong motivation for studying this problem is to understand the localization of energy along one-dimensional HB chains through protons. Most of the papers that mention HB chains or proton channels assume that such channels will transport fast and sufficiently for bioenergetic purposes [2, 11]. Recently, extensive theoretical investigations [12–16] and also some experimental evidence [17] predicted that solitons may give some answers to the fundamental question of the transmission of energy in biological macromolecules. The proton dynamics in HB chains is often modeled by a characteristic non-linear substrate potential with two degenerate equilibrium positions. The solitons ensure the transport of energy and charges in bioenergetics, e.g., mitochondrial adenosine triphosphate formation [18, 19], photophosphorylation in chloroplasts [20], anaerobic metabolism in *Halobacterium* [21], and proton migration in ice crystals [22], and explain some aspects of biological processes such as the duplication of deoxyribonucleic acid (DNA) and the transcription of messenger ribonucleic acid (mRNA) [23], the denaturation of DNA [24], and the molecular mechanism of muscle contraction [25, 26]. As a consequence, a detailed understanding of the charge transfer mechanism of HB chains will have great impact on our picture of the localization of bioenergy in HB chains.

Intrinsic localized modes (ILMs) or discrete breathers (DBs) are non-linear collective localized excitations that seem to play a very important role in various biological and physical systems. Interest in these DBs has been intensified recently due to experimental generation and observation in some chemical compounds [27, 28], antiferromagnets [29, 30], coupled arrays of Josephson junctions [31, 32], and even possibly in myoglobin [33]. Other types of non-linear systems in which DBs could possibly exist and could be detected experimentally are HB systems such as ice and quasi-one-dimensional HB chains. The formation of DBs involves no disorder and they extend over a nano-length scale similar to exact breather soliton solutions in non-linear continuum theories [34]. Pnevmatikos et al. reported on breather excitations in a one-component model for HB chains [35]. They found a

form of breathers and demonstrated numerically high-stability properties of the excitations in the case of a symmetric on-site potential. In HB chains, the power absorbed by non-linear breather modes in the presence of an external AC field is more significant than the power absorbed by the linear excitations. This effect may be useful to sufficiently analyze the non-linear properties of HB chains under external fields and to determine some of their characteristics experimentally [35]. Zolotaryuk et al. reported that a diatomic chain of heavy ions coupled by hydrogen bonds admits discrete breather solutions in the anticontinuous limit [36]. Since the study of breather-type excitations is important for the theory of protonic conductivity based on soliton phenomenology [37–43], in this paper we investigate the localization of the charge transfer in one-dimensional hydrogen-bonded (HB) chains with the nearest neighbor interactions of protons. The paper is organized as follows: In Section 2, we describe the model and derive the discrete non-linear equation of motion with the aid of the Holstein–Primakoff transformation combined with Glauber's coherent state representation. Section 3 is devoted to the analytical investigation of the modulational instability of a plane wave propagating in a proton channel of a HB chain. In Section 4, we discuss the localization of bioenergy in a HB discrete chain and demonstrate the existence of dissipative and surface mode DBs. The results are concluded in Section 5.

2 Mathematical background of proton dynamics

We consider an idealized periodic HB chain consisting of two interacting sublattices of harmonically coupled protons as shown below. Proton motion is known to be responsible for the energy and charge transfer in many HB chains [44]. The conduction via proton migration along the chain in HB systems appears as:

$$(\mathrm{H}-\mathrm{O}-\mathrm{H})^{+}\cdots\mathrm{O}-\mathrm{H}\cdots\mathrm{O}-\mathrm{H}\cdots\mathrm{O}-\mathrm{H},$$

where $(-)$ and $(\cdots)$ stand for the covalent and the hydrogen bond, respectively. The hydrogen bond bridges the system in many repetitions of the unit cell O–H$\cdots$ and the system is usually considered to be a uni-dimensional macroscopic chain. Here, H^{+} travels from one side of the chain to another by subsequent jumps of protons from one oxygen to another and finally the system becomes

$$\mathrm{H}-\mathrm{O}\cdots\mathrm{H}-\mathrm{O}\cdots\mathrm{H}-\mathrm{O}\cdots\mathrm{H}-\mathrm{O}\cdots(\mathrm{H}-\mathrm{O}-\mathrm{H})^{+}.$$

By the earlier work of Tokunaga and Matsubara [45], the Hamiltonian for the protons in a one-dimensional *xz* model of a H-bonded system in the presence of an electric field can be written in terms of spin operators as:

$$H=-2\alpha\sum_{n}S_{n}^{x}-(1/2)\,J_{1}\sum_{n}\left[S_{n}^{z}S_{n-1}^{z}+S_{n}^{z}S_{n+1}^{z}\right]-(1/2)\,J_{2}\left[S_{n}^{x}S_{n-1}^{x}+S_{n}^{x}S_{n+1}^{x}\right]-VS_{n}^{z}. \tag{1}$$

Equation (1) is written based on the idea of a quasi-spin in hydrogen-bonded systems. One half spin corresponds to the two possible positions of the proton in the double-well potential along the O–O bond (hydrogen bond). This potential is a consequence of the interaction

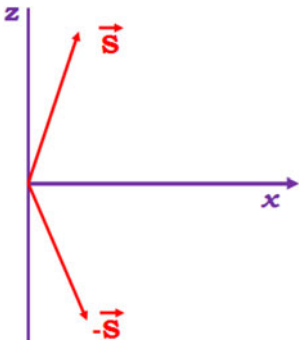

Fig. 1 The two possible orientations of the pseudospin ($\vec{s}$), which characterize the polarization vector of the H-bonded chain

between two negative ions of oxygen or some heavy ions. The discrete changes of the proton position corresponding to the two projections of spin $= (1/2)$ are represented in Fig. 1. Here, S_n^{δ} ($\delta = x, z$) are spin operators with spin magnitude S associated with the proton in the n-th H-bond. Its x-component S_n^x represents the tunneling of the n-th proton; S_n^x makes the n-th proton jump from one of the equilibrium positions a to the other equilibrium position b and vice versa (Fig. 2). S_n^z represents the polarization of the n-th H-bond and the two possible directions of S_n^z correspond to the two possible positions of the n-th proton. The first term in the right-hand side of (1) represents the kinetic energy. The second term represents the energy due to the interaction between neighboring protons. The parameter J_1 represents the strength of the interaction between protons. The terms proportional to J_2 represent the longitudinal interactions between a pair of tunneling protons and $V = q' E^z$, where q' is the charge of the proton.

The dimensionless spin operator satisfies the commutation relations $\left[S_n^+, S_m^+\right] = 2S_n^z \delta_{nm}$, $\left[S_n^{\pm}, S_m^z\right] = \mp S_n^{\pm} \delta_{mn}$ with $S_n \cdot S_n = S[S+1]$, where $S_n^{\pm} = S_n^x \pm i S_n^y$. For treating the problem semi-classically, we introduce the Holstein–Primakoff transformation [46–48] for the spin operators in terms of the bosonic operators $a_n^{\dagger}$, a_n, which satisfy the usual Bose commutation relations. At a sufficiently low-temperature limit, the ground-state expectation value of $a_n^{\dagger} a_n$ is small compared to $2S$ and n, therefore we can use the semi-classical expansions as

$$
\begin{aligned}
S_n^+ &= \sqrt{2}\left[1 - \left(\varepsilon^2/4\right) a_n^{\dagger} a_n - \left(\varepsilon^4/32\right) a_n^{\dagger} a_n a_n^{\dagger} a_n - O\left(\varepsilon^6\right)\right] \varepsilon a_n, \\
S_n^- &= \sqrt{2}\varepsilon a_n^+ \left[1 - \left(\varepsilon^2/4\right) a_n^+ a_n - \left(\varepsilon^4/32\right) a_n^+ a_n a_n^+ a_n - \mathrm{O}\left(\varepsilon^6\right)\right], \\
S_n^z &= \left[1 - \varepsilon^2 a_n^+ a_n\right], \qquad (2)
\end{aligned}
$$

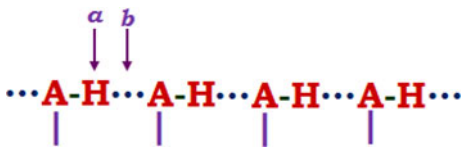

Fig. 2 Schematic representation of one-dimensional H-bonded systems

where $\varepsilon = \left(1/\sqrt{S}\right)$ and, using (2), dimension-less Hamiltonian (1) can be written in a power series of ε, as

$$
\begin{aligned}
H = & -2\sqrt{2\alpha}\left[\varepsilon\left(a_n + a_n^\dagger\right) - \left(\varepsilon^3/4\right)\left(a_n^\dagger a_n a_n + a_n^\dagger a_n^\dagger a_n\right)\right] \\
& - (1/2)\, J_1\left[2 - \varepsilon^2\left(a_{n-1}^\dagger a_{n-1} + 2a_n^\dagger a_n + a_{n+1}^\dagger a_{n+1}\right)\right. \\
& \qquad \left. + \varepsilon^4\left(a_n^\dagger a_n a_{n-1}^\dagger a_{n-1} + a_n^\dagger a_n a_{n+1}^\dagger a_{n+1}\right)\right] \\
& - J_2\left[\varepsilon^2\left(a_n a_{n-1} + a_n a_{n-1}^\dagger + a_n^\dagger a_{n-1} + a_{n-1}^\dagger a_n^\dagger + a_n a_{n+1} + a_n a_{n+1}^\dagger + a_n^\dagger a_{n+1} + a_n^\dagger a_{n+1}^\dagger\right)\right. \\
& \quad - \left(\varepsilon^4/4\right)\left(a_n a_{n-1}^\dagger a_{n-1} a_{n-1} + a_n^\dagger a_n a_n a_{n-1} + a_n a_{n-1}^\dagger a_{n-1}^\dagger a_{n-1}\right. \\
& \qquad + a_n^\dagger a_n a_n a_{n-1}^\dagger + a_n^\dagger a_{n-1}^\dagger a_{n-1} a_{n-1} + a_n^\dagger a_n^\dagger a_n a_{n-1} \\
& \qquad + a_n^\dagger a_{n-1}^\dagger a_{n-1}^\dagger a_{n-1} + a_n^\dagger a_n^\dagger a_n a_{n-1}^\dagger + a_n a_{n+1}^\dagger a_{n+1} a_{n+1} \\
& \qquad + a_n^\dagger a_n a_n a_{n+1} + a_n a_{n+1}^\dagger a_{n+1}^\dagger a_{n+1} + a_n^\dagger a_n a_n a_{n+1}^\dagger \\
& \qquad + a_n^\dagger a_{n+1}^\dagger a_{n+1} a_{n+1} + a_n^\dagger a_n^\dagger a_n a_{n+1} + a_n^\dagger a_{n+1}^\dagger a_{n+1}^\dagger a_{n+1} \\
& \qquad \left.\left. + a_n^\dagger a_n^\dagger a_n a_{n+1}^\dagger\right)\right] - q' E_z\left(1 - \varepsilon^2 a_n^\dagger a_n\right). \qquad (3)
\end{aligned}
$$

Hamiltonian (3) characterizes the low-energy non-linear property of hydrogen-bonded chains in an oblique electric field. The dynamics of the spins can be expressed in terms of the Heisenberg equation of motion for the Bose operator a_n,

$$
i\hbar\left(\frac{da_j}{dt}\right) = [a_j, H], \qquad (4)
$$

We then introduce the Glauber's coherent-state representation (p-representation) [49] defined by the product of the multimode coherent states $\left|u>=\prod_n\right| u(n)>$, with $<u|u>=1$. Each component $|u(n)>$ is an eigenstate of the annihilation operator a_n, i.e., $a_n\,|u>=u_n|\,u>$, where $|u^*(n)>$ is the coherent-state eigen vector for the operator $a_n^\dagger$ and u_n is the coherent amplitude in this representation. Since the coherent states are normalized and overcompleted, the field operators sandwiched by $|u(n)>$ can be represented only by their diagonal elements. The p-representation of the non-linear equation leads to

$$
\begin{aligned}
& i\frac{\partial u_n}{\partial t} + 2\sqrt{2\alpha}\left[\varepsilon - \left(\varepsilon^3/4\right)\left(u_n^2 + 2\,|u_n|^2\right)\right] - J_1\left[-2\varepsilon^3 u_n + \varepsilon^4 u_n\left(|u_{n+1}|^2 + |u_{n-1}|^2\right)\right] \\
& \quad - (J_2/2)\left[\left(2\varepsilon^2 - \varepsilon^4 u_n^2 - 2\varepsilon^4\,|u_n|^2\right)\left(u_{n+1} + u_{n-1} + u_{n+1}^* + u_{n-1}^*\right)\right. \\
& \qquad \left. - \varepsilon^4\,|u_{n+1}|^2\left(u_{n+1} + u_{n+1}^*\right) - \varepsilon^4\,|u_{n-1}|^2\left(u_{n-1} + u_{n-1}^*\right)\right] \\
& \quad + q' E_z \varepsilon^2 u_n = 0. \qquad (5)
\end{aligned}
$$

The above discrete equation contains various non-linear couplings and they lead to different non-linear phases, which are represented by various types of non-linear excitations. Equation (5) is difficult to solve due to its non-linearity and discreteness. In addition, the discreteness makes the properties of the system periodic, so that due to the interplay between the discreteness and non-linearity, new types of non-linear excitations, which are absent in continuum models, may be possible in the system.

3 Discrete solitons via modulational instability

Wave instabilities are probably the most remarkable non-linear phenomena that may occur in nature [50]. One of the first instabilities discovered for non-linear models was the modulational instability, which is known to be an effective physical mechanism in fluids [51] and optics [52–54] for the breakup of continuous modes into discrete solitary localized modes. Discrete models are of great interest for practical applications such as models for energy transport in biophysical systems proposed by Davydov [55], systems that model the dynamics of DNA [56], discrete reaction–diffusion models to study propagation failure in myocardial tissue [57], myelinated axons [58, 59], and discrete quantum motors [60, 61]. The diversity of these models and their richness compared to those in continuous systems are essentially due to the mutual interplay of the peculiar transport properties such as proton tunneling in HB chains. In this respect, the non-linear properties of HB chains under an external field and the relevant localization phenomenon deserve particular attention because the interaction between two neighboring protons happens at different frequencies and new degrees of freedom enter into the dynamical process.

In this section, the modulational instability of a plane wave in a proton channel is investigated by studying the stability of its amplitude in the presence of a sufficiently small perturbation so that one can linearize the equation for the envelope and the carrier wave. Looking for the slow modulation of a carrier wave that has its frequency in the linear frequency band, we invoke the rotating wave approximation (RWA) to the discrete equation of motion (5):

$$\begin{aligned} i\dot{\phi}_n &+ \left(\omega_0 + 2J_1\varepsilon^2 - q' E_z \varepsilon^2\right)\phi_n - J_1\varepsilon^4\left[2\phi_n\left(|\phi_{n+1}|^2 + |\phi_{n-1}|^2\right) + \phi_n^*\left(\phi_{n+1}^2 + \phi_{n-1}^2\right)\right] \\ &- J_2\left[2\varepsilon^2\left(\phi_{n+1} + \phi_{n-1}\right) - \varepsilon^4\left[\phi_n^2\left(\phi_{n+1}^* + \phi_{n-1}^*\right) + 2|\phi_n|^2\left(\phi_{n+1} + \phi_{n-1}\right)\right.\right. \\ &\left.\left. + 3|\phi_{n+1}|^2\phi_{n+1} + 3|\phi_{n-1}|^2\phi_{n-1}\right]\right] = 0. \end{aligned} \tag{6}$$

In order to investigate how weakly the time-dependent perturbations evolve along the HB chain, we perform the following linear stability analysis. The steady-state solution of (6) is given by

$$\phi_n = \phi_0 e^{i(kn - wt)}, \tag{7}$$

where wavenumber k, angular frequency ω and amplitude ϕ_0 satisfy the following dispersion relation:

$$\omega = 2\varepsilon^4\phi_0^2\left[J_1\left(1 + \cos 2k\right) + 6J_2\cos k\right] - \omega_0 - 2J_1\varepsilon^2 + q' E_z\varepsilon^2 + 4J_2\varepsilon^2\cos k. \tag{8}$$

The linear stability analysis of the steady state can be examined by introducing the perturbed field of the form

$$\phi_n = (\phi_0 + \delta\phi_n)\, e^{i(kn-\omega t)}, \tag{9}$$

where $\delta\phi_n$ is assumed to be a small perturbation in comparison with the carrier wave amplitude ϕ_0. The equation that describes the evolution of the perturbation is given by

$$\begin{aligned} i\dot{\delta\phi}_n &+ \left(\omega + \omega_0 + 2J_1\varepsilon^2 - q' E_z \varepsilon^2\right)\delta\phi_n \\ &- J_1\varepsilon^4\phi_0^2\left[2\left(\delta\phi_{n+1} + \delta\phi_{n-1} + 2\delta\phi_n + \delta\phi_{n+1}^* + \delta\phi_{n-1}^*\right)\right. \\ &\left. + 2\delta\phi_{n+1}e^{2ik} + 2\delta\phi_n^*\cos 2k + 2\delta\phi_{n-1}e^{-2ik}\right] \\ &- J_2\left[2\varepsilon^2\left(\delta\phi_{n+1}e^{ik} + \delta\phi_{n-1}e^{-ik}\right)\right. \\ &-\varepsilon^4\phi_0^2\left(2\delta\phi_{n+1}^*\cos k + 2\delta\phi_{n-1}^*\cos k + 8\delta\phi_n\cos k + 8\delta\phi_{n+1}e^{ik}\right. \\ &\left.\left. + 8\delta\phi_{n-1}e^{-ik} + 4\delta\phi_n^*\cos k + 2\delta\phi_{n+1}^*e^{ik} + 2\delta\phi_{n-1}^*e^{-ik}\right)\right], \end{aligned} \tag{10}$$

where the asterisk denotes the complex conjugate. Thus, if the perturbed field grows exponentially, the steady state becomes unstable. We assume a general solution of the form

$$\delta\phi_n = \phi_1 e^{i(qn-\Omega t)} + \phi_2^* e^{-i(qn-\Omega^* t)}, \tag{11}$$

where q and Ω represent the wavenumber and angular frequency of the perturbation, respectively, and ϕ_1 and ϕ_2^* are the complex constant amplitudes. Inserting (11) into (10), we obtain

$$\begin{pmatrix} \Omega + A^+ & B^+ \\ B^- & -\Omega + A^- \end{pmatrix}\begin{pmatrix} \phi_1 \\ \phi_2 \end{pmatrix} = \begin{pmatrix} 0 \\ 0 \end{pmatrix}, \tag{12}$$

where

$$\begin{aligned} A^\pm = &\left(\omega + \omega_0 + 2J_1\varepsilon^2 - q' E_z\varepsilon^2\right) - 2J_1\varepsilon^4\phi_0^2\left(1 + 2\cos q + 2\cos\left(2k \pm q\right)\right) \\ &- 4J_2\left[\varepsilon^2\cos\left(k \pm q\right) + 2\varepsilon^4\left(\cos k + 2\cos\left(k \pm q\right)\right)\right], \\ B^\pm = &-2J_1\varepsilon^4\phi_0^2\left(\cos 2k + \cos q\right) + 4J_2\varepsilon^4\phi_0^2\left(\cos k + 2\cos\left(k \pm q\right)\right), \end{aligned}$$

which has the solution

$$\begin{aligned}
\Omega = {} & J_1\varepsilon^4\phi_0^2\left[1+2\cos q+2\cos(2k+q)\right] \\
& +2J_2\left[\varepsilon^2\cos(k+q)+2\varepsilon^4\left[\cos k+2\cos(k+q)\right]\right] \\
& -J_1\varepsilon^4\phi_0^2\left[1+2\cos q+2\cos(2k-q)\right] \\
& -2J_2\left[\varepsilon^2\cos(k-q)+2\varepsilon^4\left[\cos k+2\cos(k-q)\right]\right] \\
& +(1/2)\left\{\left[-2J_1\varepsilon^4\phi_0^2\left[1+2\cos q+2\cos(2k+q)\right]\right.\right. \\
& \quad -4J_2\left[\varepsilon^2\cos(k+q)+2\varepsilon^4\left(\cos k+2\cos(k+q)\right)\right] \\
& \quad +2J_1\varepsilon^4\phi_0^2\left[1+2\cos q+2\cos(2k-q)\right] \\
& \quad \left.\left.+4J_2\left[\varepsilon^2\cos(k-q)+2\varepsilon^4\left(\cos k+2\cos(k-q)\right)\right]\right] \\
& \quad -4\left[-2J_1\varepsilon^4\phi_0^2\left(\cos 2k+\cos q\right)+4J_2\varepsilon^4\phi_0^2\left(\cos k+2\cos(k+q)\right)\right] \\
& \quad -\left[2J_1\varepsilon^4\phi_0^2\left(\cos 2k+\cos q\right)+4J_2\varepsilon^4\phi_0^2\left(\cos k+2\cos(k-q)\right)\right] \\
& \quad +4\left[\omega+\omega_0+2J_1\varepsilon^2-q'E_z\varepsilon^2-2J_1\varepsilon^4\phi_0^2\left(1+2\cos q+2\cos(2k+q)\right)\right. \\
& \qquad \left.-4J_2\left[\varepsilon^2\cos(k+q)+2\varepsilon^4\left(\cos k+2\cos(k+q)\right)\right]\right] \\
& \quad \times\left[\omega+\omega_0+2J_1\varepsilon^2-q'E_z\varepsilon^2-2J_1\varepsilon^4\phi_0^2\left(1+2\cos q+2\cos(2k-q)\right)\right. \\
& \qquad \left.\left.-4J_2\left[\varepsilon^2\cos(k-q)+2\varepsilon^4\left(\cos k+2\cos(k-q)\right)\right]\right]\right\}^{(1/2)}. \qquad (13)
\end{aligned}$$

Therefore, the modulational instability (MI) gain is represented as

$$g(\Omega) = 2\,Im(\Omega). \qquad (14)$$

The steady-state solution becomes unstable whenever $\Omega < 0$ since the perturbation grows exponentially with the intensity given by the growth rate or the MI gain. The gain in (14) shows the interesting dependence of Ω on the coupling parameters J_1, J_2 and the applied electric field. Equation (14) determines the stability and instability of a plane wave with wavenumber q in discrete HB chains. We study the linear stability analysis using the realistic values of parameters J_1, J_2 and ω_0. Thus, we investigate the effects of the tunneling motion of the proton and the interaction between two neighboring protons on localization, and we demonstrate that the features of these coupling coefficients are able to qualitatively affect the stability properties. Linear stability analysis can determine the instability domain in parameter space and predicts qualitatively how the amplitude of a modulation sideband evolves at the onset of the instability.

Figures 3 and 4 depict the regions of stability/instability and the corresponding dependence of the growth rate on the wavenumbers q and k for the various values of J_1 and J_2, respectively. The pictorial representation of Figs. 3 and 4 explores the impact of the coupling between the nearest-neighbor proton–proton interaction on the stability/instability regime of HB chains. In the figures, the dark bluish area corresponds to a region where the non-linear plane waves are stable with respect to the modulation of any wavenumber q and the bright yellow-orange region experiences more instability in which the amplitude of any wave would be expected to suddenly display an exponential growth. Using the

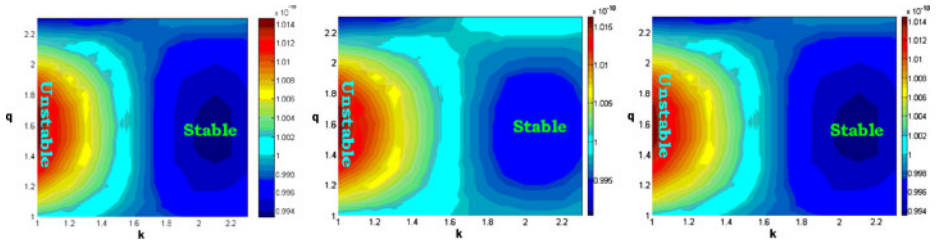

Fig. 3 Gain spectrum for $J_1 = 1.2$, 1.3 and $1.5 \cdot 10^{-19}$ J. On all plots, $\omega_0 = 10^{-15}$, $J_2 = 1 \cdot 10^{-19}$ J, $q' = 1.6 \cdot 10^{-19}$ C, $E_z = 1$ Vm^{-1}, $\varepsilon = 1.93$ and $\phi_0 = 10.8$

fundamental parameters of the HB chain, we have plotted the growth rate $g(\Omega)$ by choosing the parameters $\omega_0 = 10^{-15}$, $J_2 = 1 \cdot 10^{-19}$ J, $q = 1.6 \cdot 10^{-19}$ C, $E_z = 1$ Vm^{-1}, $\varepsilon = 1.93$ and $\phi_0 = 1.8$ and by varying the value of J_1 from (0.2–0.7) $\cdot$ 10^{-19} J. In Fig. 5, the plot of the gain profile depicts the periodic and coherent breathing of the peaks with $J_1 = 0.2 \cdot 10^{-19}$ J becoming more persistent as J_1 increases.

When the value of J_1 varies, these localized peaks merge into stronger ones while radiating as low-amplitude waves. The periodic pattern becomes modulated so that the gaps between the initially equidistant peaks begin to vary. Figure 5 shows the tiny variations in this distance as the peaks start to move at $J_1 = 0.4 \cdot 10^{-19}$ J. The most important phenomenon following the phase instabilities is the formation of stable structures through merging of localized peaks. Once the coupling between the polarization of the n-th and $(n + 1)$-st H-bond increases, peaks that are situated remotely from the first merge together to become a more persistent one so that they are traced by continuous lines, thus subsequently driving the HB chain to be more stable against perturbations, as is confirmed by their corresponding density plots as shown in Fig. 3.

Surprisingly, when the value of J_2 is increased, the HB chain drives slowly from a stable state to an unstable state as depicted in Fig. 4. From Fig. 4, we explain this special feature by the fact that the size of the stability zone slowly decreases as the value of J_2 increases and the simulations confirm the prediction of the instability when a modulated wave moves in the HB chain with a non-vanishing imaginary part of the frequency of the modulated wave, leading back to the formation of localized breathing coherent structures as shown in Fig. 6. Further, an increase in the value of an applied electric field (see Fig. 7) does not significantly disturb the periodic evolution of the coherent modes; rather, it produces a small decrement in the amplitude of the modes. These results confirm that the protonic transport

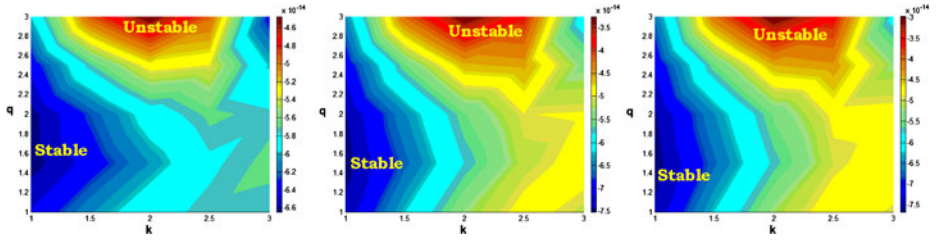

Fig. 4 Gain spectrum for $J_2 = 1.0$, 6.0 and $9.0 \cdot 10^{-19}$ J. On all plots, $\omega_0 = 10^{-15}$, $J_1 = 1 \cdot 10^{-19}$ J, $q' = 1.6 \cdot 10^{-19}$ C, $E_z = 1$ Vm^{-1}, $\varepsilon = 1.93$ and $\phi_0 = 10.8$

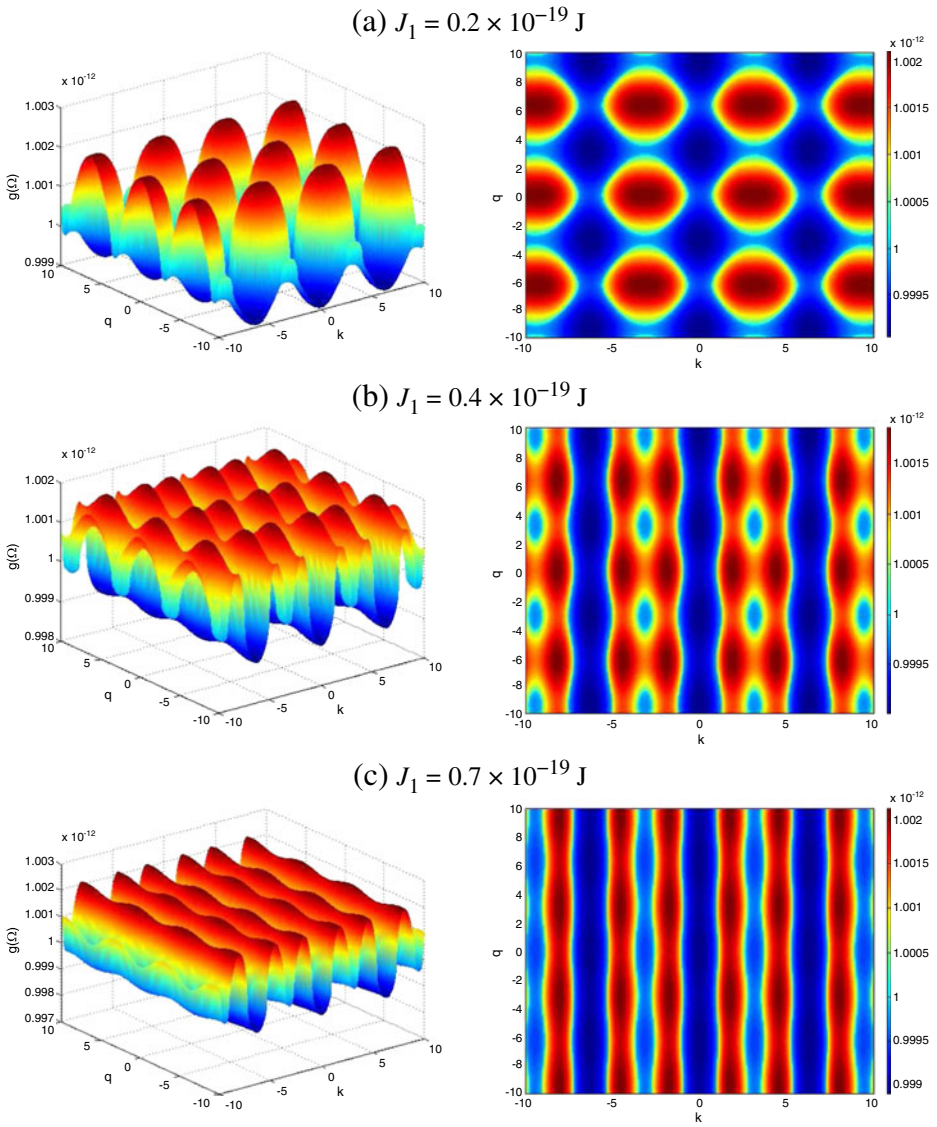

Fig. 5 Growth rate of the HB system for various values of J_1. On all plots, $\omega_0 = 10^{-15}$, $J_2 = 1 \cdot 10^{-19}$ J, $q' = 1.6 \cdot 10^{-19}$ C, $E_z = 1$ Vm^{-1}, $\varepsilon = 1.93$ and $\phi_0 = 1.8$

is very sensitive and depends entirely on the competition between the two interactions characterized by the parameters J_1 and J_2.

4 Molecular dynamical simulations

In order to check the validity of our analytical approach and to determine the evolution of the system by taking into account the instability zone, we perform molecular dynamics

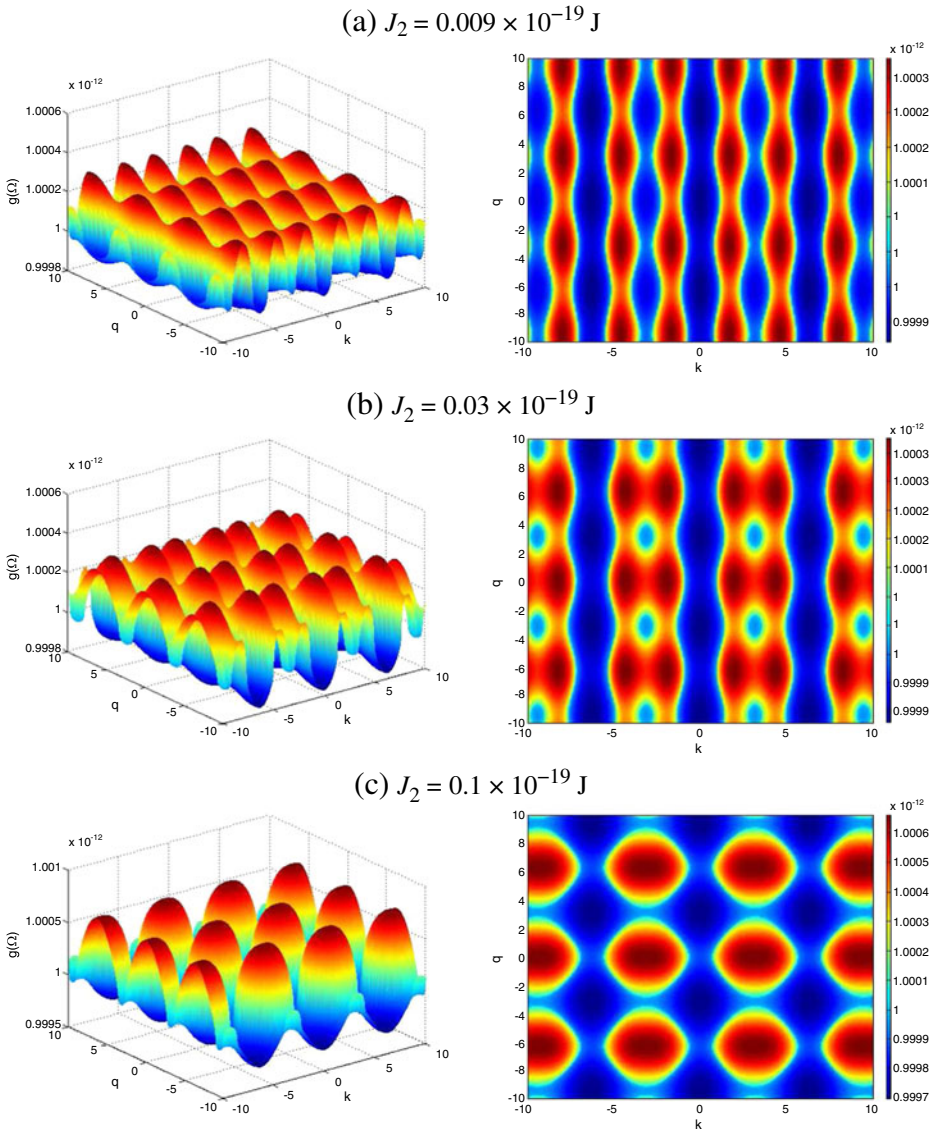

Fig. 6 Growth rate of the HB system for various values of J_2. On all plots, $\omega_0 = 10^{-15}$, $J_1 = 1 \cdot 10^{-19}$ J, $q' = 1.6 \cdot 10^{-19}$ C, $E_z = 1$ Vm^{-1}, $\varepsilon = 1.93$ and $\phi_0 = 1.8$

(MD) numerical simulations on (5) using the fourth-order Runge–Kutta method. As an extension of the analytical approach of the modulational instability, it is important to treat the discreteness completely, especially when both the carrier wave and the envelope cannot be described in terms of long-wavelength components. Though the modulational instability of protonic transport in a HB chain has been deduced from the linear stability analysis, such analysis is based only on the linearization around the unperturbed carrier wave. At a large time scale, the analysis neglects the additional combination of waves generated

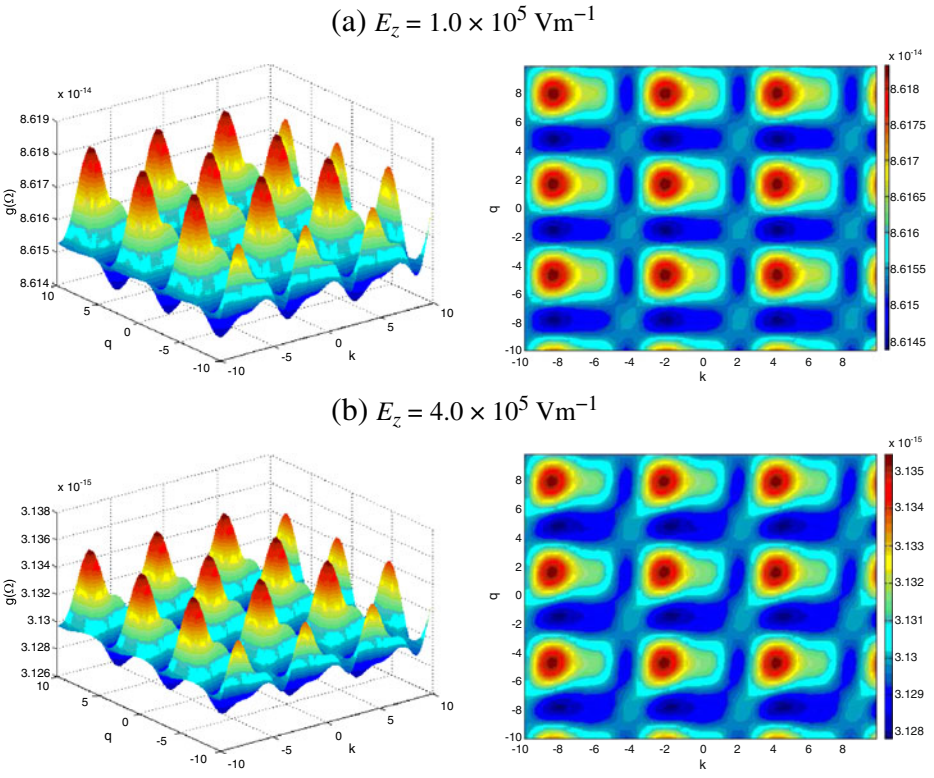

Fig. 7 The instability gain versus the modulation wavenumber k and the amplitude of the continuous wave in the unstable regime for various values of E_z. On all plots, $\omega_0 = 10^{-15}$, $J_1 = 1 \cdot 10^{-19}$ J, $J_2 = 1 \cdot 10^{-19}$ J, $q' = 1.6 \cdot 10^{-19}$ C, $\varepsilon = 1.93$ and $\phi_0 = 1.8$

through wave mixing processes, which becomes significant if the wave vector falls inside an instability domain. Thus, at the long time scale, the evolution of the modulated extended non-linear waves can be well explored by molecular dynamics simulations. In these simulations, the energy scaling in the microcanonical ensemble represents $H^{\max} \propto N^2$, where N is the norm. Also, we use a time scale with $t = \frac{T_{SWF}}{S_c}$ i.e., $t \approx \frac{T_{SWF}}{S\hbar}$ as the unit of time and $S_c = S\hbar$, where S is the spin length and $\hbar$ is the Planck constant. Here T_{SWF} denotes the period of the spin wave that can be derived from the frequency given in the dispersion relation of (8).

When the instability is fully developed, the formation of localized modes can be determined by MD numerical simulations. The MD simulation is performed with a chain of $N = 200$ units with periodic boundary conditions, so that the wave vector k is defined as modulo 2π in the lattice and chosen in the form $k = (2\pi p/N)$ and $q = (2\pi P/N)$, where $p(P)$ is an integer lower than $(N/2)$. The initial conditions of the modulated plane wave are written as

$$\begin{aligned} u_n\,(t=0) &= [u_0 + 0.01 \quad \cos(qn)] \quad \cos(kn)\,, \\ \dot{u}_n\,(t=0) &= [u_0 + 0.01 \quad \cos(qn)] \quad \omega \sin(kn)\,, \end{aligned} \tag{15}$$

and we study the behavior of the modulated wave with the help of a discrete spatial Fourier transform of $u_n(t)$. In order to monitor the time evolution of individual Fourier components, we define the complete spatial Fourier transform of the wavefunction as

$$S_p(t) = \sum_{n=0}^{N-1} u_n(t) \exp\left[(i2\pi p/N)\right], \quad \text{with} \quad 0 \leq p \leq (N/2). \tag{16}$$

It is to be noted that $S_p(t) =< a_n(t) >$ is the expectation value of the boson operator, which is proportional to the transverse value of the proton polarization $S_n^+ = S_n^x + iS_n^y$ and thus represents the proton transfer amplitude.

First, we attempt to investigate the short-time instability in a HB chain of 200 units with periodic boundary conditions. In order to analyze precisely the instability of a given wave, we must not only consider the applied modulation q but also the modulation arising from the non-linear term and their contribution modes in the simulations. Figure 8 depicts the complete Fourier spectrum on which we observe the instability as predicted in Figs. 3 and 4, for the wavenumbers $(k, q) = ((43\pi/64), (33\pi/64))$. Figure 8a portrays the evolution of a carrier wave with $(k, q) = ((43\pi/64), (33\pi/64))$ for about 300 units of time. From Fig. 8 it is evident that none of the $k \pm q$ satellite side bands display any stability. Even the higher harmonics of the modulation satellite side bands illustrate the origin of the oscillatory instability. Thus the analytical prediction of instability is effectively verified numerically in the log-linear plots of Fig. 8a.

When we investigate the evolution of the carrier wave for a sufficiently larger time $t = 600$, a higher instability is induced by the modulation of the carrier wave with the wavenumbers $(k, q) = ((43\pi/64), (33\pi/64))$ along with the system parameters as shown in Fig. 8b. We have found that the oscillatory instability in the satellite bands leads to localization in the discrete HB chain. We also investigate the evolution of the carrier wave for a sufficiently larger time $t = 900$ and eventually a higher instability is induced by the modulation of the carrier wave with the wavenumbers $(k, q) = ((43\pi/64), (33\pi/64))$ along with the system parameters as shown in Fig. 8c. Thus the stronger non-linear coupling for a long time in the presence of other combination modes $2q, 3q, ...k \pm q$, along with the principal satellite modulation $k \pm q$, triggers localization of long-lived excitations in the presence of low-amplitude noise with suitable wavenumbers, as shown in Fig. 8. Furthermore, it is now possible to create localized excitations in a HB chain with our approach of modulational instability. Figure 8 shows how the time evolution of the complete spectrum along with the additional combination modes generated from wave-mixing processes leads to the localized non-linear modes in a discrete HB chain. From all the log-Fourier plots, it is evident that, although the amplitudes of most of the Fourier components of some principal modes $k \pm q$ initially increase at a slow rate, the $3q$ modulation is the one that rapidly triggers the zigzag instability in the system. This can be understood by the fact that, though the linear-stability analysis neglects the additional satellite bands generated through wave-mixing processes, they become significant and drive the system into a chaotic regime at a larger time scale if their wavevector falls into an unstable zone. Hence, needless to mention, these molecular dynamics simulations demonstrate that a HB chain, with a set of fundamental parameters, can support the long-lived excitations that are excited through modulational instability processes.

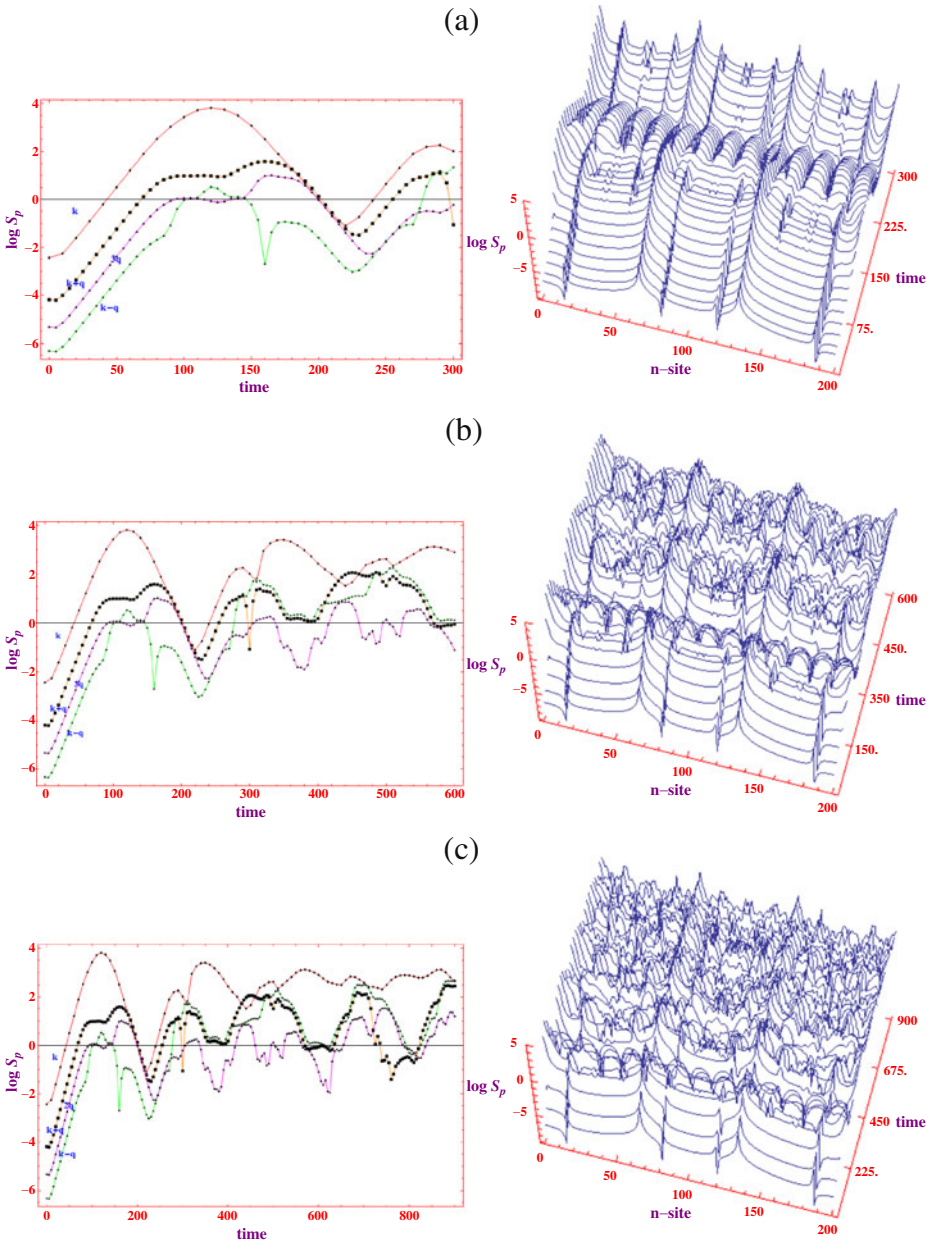

Fig. 8 Time evolution of the Fourier components and the complete spatial Fourier spectrum of the wave for $\alpha = 0.16$, $J_1 = 0.19 \cdot 10^{-19}$ J, $J_2 = 0.15 \cdot 10^{-19}$ J, $q' = 1.6 \cdot 10^{-19}$ C, $E_z = 1.2$ Vm^{-1}, $k = (43\pi/64)$, $q = (33\pi/64)$, (**a**) $t = 300$, (**b**) $t = 600$ and (**c**) $t = 900$

5 Localization of energy

It has been demonstrated by Lai and Sievers [62] that, in an antiferromagnetic spin chain, a delocalized state in Fourier space can either be a localized state or a delocalized state in the

corresponding real space, depending on the relative phases between Fourier components; the time evolution in Fourier space alone does not tell us the complete process of energy distribution. However, it is generally believed that the system will finally reach equipartition of energy over a sufficiently long time since entropy should grow during the system's time evolution.

Here we investigate the evolution of energy density and the role of nearest-neighbor proton–proton interactions on the localization of energy along the HB chains. Previous studies suggest the physical system should approach a state where the energy is evenly distributed not only among the modes in Fourier space but also on lattice sites in real space. The results of the modulational instability suggest that when plane waves are highly unstable, it leads to the formation of spatially localized structures. This MI-induced energy localization has been proposed to be the mechanism responsible for the formation of intrinsic localization by many authors [63–69]. The normalized energy density distribution is represented by

$$\begin{aligned} e(n) = \sum_n \Big[& -\sqrt{2\alpha}\left[\varepsilon u_n^* - \left(\varepsilon^3/4\right)\left(|u_n|^2 u_n + |u_n|^2 u_n^*\right) - \left(\varepsilon^5/32\right)\left(|u_n|^4 u_n + |u_n|^4 u_n^*\right)\right] \\ & - J_1\left[-2\varepsilon^2 |u_n|^2 + \varepsilon^4 |u_{n+1}|^2 |u_n|^2\right] + J_2\varepsilon^2\left(u_{n+1}u_n^* + u_n u_{n+1}^* + u_{n+1}^* u_n\right) \\ & - J_2\varepsilon^4\left[u_{n+1}|u_n|^2 u_n^* + u_{n+1}^*|u_n|^2 u_n^* + u_{n+1}^*|u_n|^2 u_n + |u_{n+1}|^2 u_{n+1}^* u_n \right. \\ & \left. + |u_{n+1}|^2 u_{n+1}^* u_n^* + u_{n+1}^2 u_n^* u_{n+1}^* + u_{n+1}|u_n|^2 u_n + u_{n-1}|u_n|^2 u_n\right] \\ & + q' E_z \varepsilon^2 |u_n|^2 \Big]. \end{aligned} \tag{17}$$

We perform the MD simulations by considering a HB chain of 200 units of atoms to compute the energy-density distribution defined by (17) and analyze the role of proton–proton interaction parameters with the same considerations. Figure 9 depicts the evolution of energy density for various values of the neighboring proton–proton interaction strength J_1 for about 1,000 units of time with periodic boundary conditions. Figure 9a, b portrays the creation of intrinsic localized excitations via modulational instability and time evolution of the energy density distribution in real space. From Fig. 9a it is evident that when $J_1 = 0.192 \cdot 10^{-19}$ J at $t = 0$, the uniform mode of the wave band is excited with a specific amplitude. We find that for $t < 250$, the large amplitude uniform mode is stable and after this it breaks up into DBs that are fairly uniformly spaced with a spatially periodic pattern. Surprisingly, it should be noted that when the value of J_1 is increased, the instability breaks up faster than the previous case and a similar breakup of the uniform mode happens even at $t = 215$ when $J_1 = 0.5 \cdot 10^{-19}$ J as shown in Fig. 9b. Thus it is confirmed that the role of the interaction between the neighboring protons affects the breakup of the uniform mode into highly localized DBs along the HB chain.

A contrary trend is observed when J_2, the interaction between the tunneling neighboring protons, is increased from $J_2 = 0.19 \cdot 10^{-19}$ J to $J_2 = 2.0 \cdot 10^{-19}$ J (Fig. 10a) and it is also observed that the large amplitude uniform mode breaks up into localized DBs at $t = 75$. Eventually, an increase in the value of J_2 delays the breakup and the energy flows in the spatially and temporally periodic DBs as confirmed by Fig. 10b with a further delayed breakup at $t = 200$. It is evident that the interaction parameter J_1 hastens the breakup of the large-amplitude uniform mode into non-linear oscillating DBs in contrast to J_2, which in principle delays the breakup process.

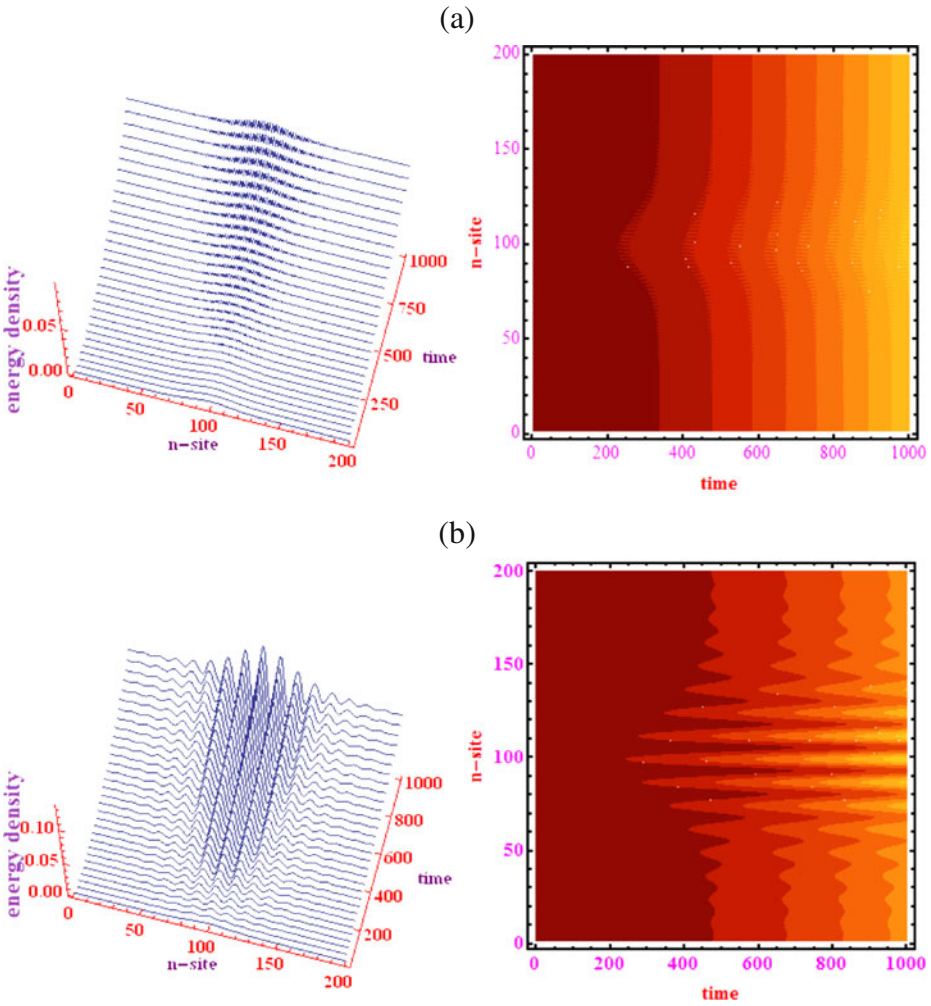

Fig. 9 Long-term evolution of the energy density along the chain for $J_2 = 0.53 \cdot 10^{-19}$ J, $\alpha = 0.021$, $q' = 1.6 \cdot 10^{-19}$ C, $E_z = 0.3$ Vm^{-1}, (**a**) $J_1 = 0.192 \cdot 10^{-19}$ J and (**b**) $J_1 = 0.5 \cdot 10^{-19}$ J

The adjacent two-dimensional contour plots display the evolution of the energy at each site as a function of site of the n-th proton and time. In the contour plots, the brighter yellow region identifies the higher energy excited modes of DBs and the darker area refers to the minimum or zero energy of the proton. Thus we demonstrate the formation of localized coherent structures numerically and the role of the interaction parameters J_1 and J_2. It is worth noting that the interaction parameters of the neighboring protons effectively influence the energy density distribution along the HB chains and thus promote the charge transport in a lossless way. It can also be realized that the lifetime of the DB is increased until 1,000 units of time upon tuning of the proton–proton interaction in the HB chains.

We aim to construct the DBs numerically in the framework of the one-dimensional model of hydrogen-bonded chains. These localized non-linear oscillating breather solutions

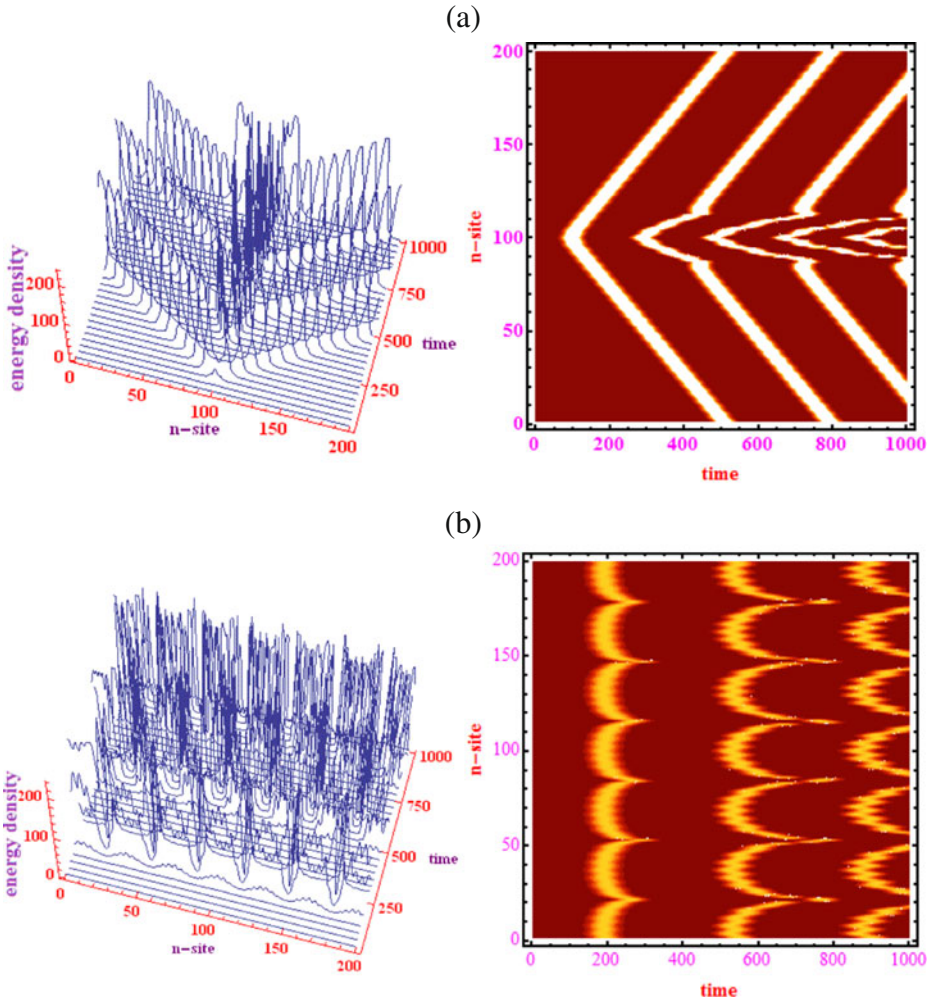

Fig. 10 Long-term evolution of the energy density along the chain for $J_1 = 0.79 \cdot 10^{-19}$ J, $\alpha = 0.021$, $q' = 1.6 \cdot 10^{-19}$ C, $E_z = 0.3$ Vm^{-1}, (**a**) $J_2 = 0.19 \cdot 10^{-19}$ J and (**b**) $J_2 = 2.0 \cdot 10^{-19}$ J

play an important role in the transport properties of hydrogen-bonded chains [36–43]. The computational tools for studying DB properties are confined to the case of a finite lattice size. We construct the DBs in a discrete hydrogen-bonded chain through numerical simulations using a Newton–Raphson scheme. According to the simplest version of this method, one looks for the stationary wave solutions in the form of $u_n(t) = u_n e^{i\gamma t}$, where γ is the non-linearity-induced shift of the propagation constant. Our numerical calculation is made at $n = 41$ atoms and we seek localized modes in the form of DBs by varying the values of γ. Figure 11 depicts snapshots of the non-linear oscillating discrete breather modes centered at different proton sites in HB chains near the surface for various values of the parameter γ. In Fig. 11, the DBs shown are highly localized and they assume their bulk form within a distance of a few lattice sites from the surface, so that the DBs shown

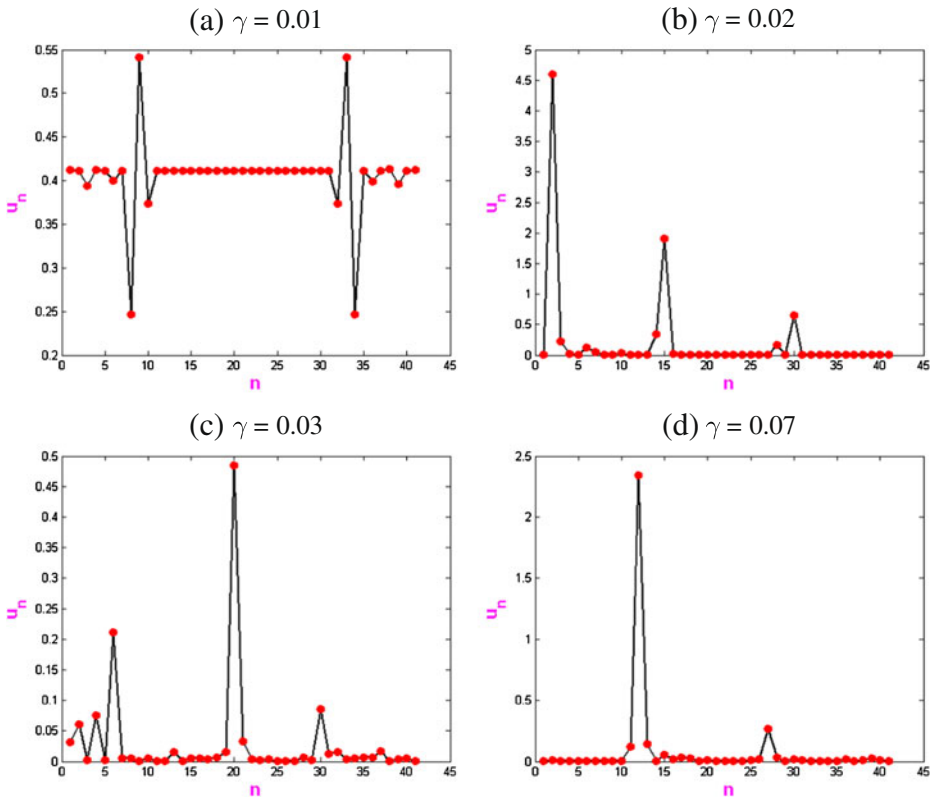

Fig. 11 Snapshots of intrinsic surface modes with stationary multisite bulk breathers in hydrogen-bonded chains. (**a**) Asymmetric DB, (**b** and **c**) symmetric surface mode DBs and (**d**) symmetric double peaked DBs. On all plots $J_1 = 3.51 \cdot 10^{-19}$ J, $J_2 = 0.19 \cdot 10^{-19}$ J, $\alpha = 0.5$, $q' = 1.6 \cdot 10^{-19}$ C, $\varepsilon = 1.4$ and $E_z = 5.4$ Vm^{-1}

in Fig. 11 can be considered as bulk multisite breather modes. Upon tuning the initial conditions appropriately, we obtain the three-site antisymmetric bulk DBs with a non-zero amplitude at all sites of HB chains when $\gamma = 0.01$, as shown in Fig. 11a. In contrast to Fig. 11a, when $\gamma = 0.02$, we observe dissipative single-site multi-surface breather profiles appearing one layer away from the surface as shown in Fig. 11b and similar single-site surface breather profiles are observed for the value of $\gamma = 0.03$ as shown in Fig. 11c. In Fig. 11c, the central atom performs a large amplitude oscillation and the nearest neighbors enjoy small amplitude oscillations. The bio-energy distribution among the DBs is shown in Fig. 11d when $\gamma = 0.07$. Here, essentially in the higher amplitude, DB five lattice sites are involved in the motion, hence we find a rather localized DB in the nanoscale length range. Generally, even for a moderate amount of perturbation, the DBs retain their localized shape and support long-lived coherent proton transfer along the strands of HB chains.

When considering larger time scales compared to the breather period, the mere linear stability of a breather no longer guarantees the eternal existence of the breathers in the presence of a small perturbation and there are still many questions open concerning the various mechanisms by which breathers may grow or decay, or possibly finally be

destroyed. If the breathers have a finite lifetime, the determination of this lifetime is of larger importance for understanding the role of breathers in real systems. An important property of the discrete breather is the so-called targeted energy transfer, which means that, under some condition, a very selective vibrational energy transfer between discrete breathers from one part of the system to another can occur. Therefore, in order to better understand the importance of discrete breathers in physical problems, it is necessary to study their fundamental properties such as their existence and stability for systems with a more sophisticated spatial symmetry and structure. In this mechanism, energy could be transferred between far distances but across specific sites that are weakly coupled. The idea is that a purely non-linear interaction supports a faster energy transfer than the exponential spatial decay of breathers.

6 Conclusions

Hydrogen bonds are the glue of life. There is a fundamental non-linearity associated with the presence of hydrogen bonding that stems from the nature of the bond itself. In this paper, we have presented a simplified model for bioenergy transport in one-dimensional HB chains with nearest-neighbor proton interactions. We have investigated the modulational instability both analytically in the framework of linear stability analysis and numerically by means of molecular dynamics (MD) simulations. The linear stability analysis predicted the stability/instability regions and the growth rates of modulation satellites. Our MD simulations demonstrate that the analytical predictions correctly describe the onset of instability. Since linear stability analysis fails for longer time scales, numerical simulation is employed. Our MD simulations have demonstrated that, with appropriate choices of interaction parameters J_1 and J_2, it is possible to create long-lived localized non-linear excitations in the form of DBs.

Acknowledgements One of the authors, L. K., gratefully acknowledges the financial support from UGC, NBHM, India, in the form of major research projects, BRNS, India, in the form of a Young Scientist Research Award and ICTP, Italy, for a Junior Associateship. A. M. gratefully acknowledges UGC for the Rajiv Gandhi National Fellowship. This research work was partially supported by Serbian Ministry of Education and Sciences (grant III45010).

References

1. Papa, S.: Molecular mechanism of proton translocation by the cytochrome system and the ATPase of mitochondria. Role of proteins. J. Bioenerg. Biomembr. **14**, 69–86 (1982)
2. Buch-Pedersen, M.J., Pedersen, B.P., Veierskov, B., Nissen, P., Palmgren, M.G.: Protons and how they are transported by proton pumps. Pflügers Arch.-Eur. J. Physiol. **457**, 573–579 (2009)
3. Whitehead, S.J., Iwaki, M., Cotton, N.P., Rich, P.R., Jackson, J.B.: Inhibition of proton-transfer steps in transhydrogenase by transition metal ions. Biochim. Biophys. Acta **1787**, 1276–1288 (2009)
4. Pedersen, A., Karlsson, G.B., Rydström, J.: Proton-translocating transhydrogenase: an update of unsolved and controversial issues. J. Bioenerg. Biomembr. **40**, 463–473 (2008)
5. Schultz, B.E., Chan, S.I.: Structures and proton-pumping strategies of mitochondrial respiratory enzymes. Annu. Rev. Biophys. Biomol. Struct. **30**, 23–65 (2001)
6. Jormakka, M., Byrne, B., Iwata, S.: Protonmotive force generation by a redox loop mechanism. FEBS Lett. **12**, 25–30 (2003)
7. Berry, M.N.: The function of energy-dependent redox reactions in cell metabolism. FEBS Lett. **117**, K106–K120 (1980)
8. Berry, M.N.: An electrochemical interpretation of metabolism. FEBS Lett. **134**, 133–138 (1981)

9. Nagle, J.F., Mille, M., Morowitz, H.J.: Theory of hydrogen-bonded chains in bioenergetics. J. Chem. Phys. **72**, 3959(1–13) (1980)
10. Blair, D.F.: Flagellar movement driven by proton translocation. FEBS Lett. **545**, 86–95 (2003)
11. Yomosa, S.: Dynamics of the protons in one-dimensional hydrogen-bonded systems. J. Phys. Soc. Jpn. **51**, 3318–3324 (1982)
12. Hennig, D., Neißner, C., Velarde, M.G., Ebeling, W.: Effect of anharmonicity on charge transport in hydrogen-bonded systems. Phys. Rev. B **73**, 024306(1–10) (2006)
13. Sinkala, Z.: Soliton/exciton transport in proteins. J. Theor. Biol. **241**, 919–927 (2006)
14. Takasu, I., Sugawara, T., Mochida, T.: Dielectric response in bisquaric acid crystal: possible generation of protonic soliton in a quasi-one-dimensional hydrogen-bonded system. J. Phys. Chem. B **108**, 18495–18499 (2004)
15. Xu, J.-Z.: Soliton dynamics in the helix polypeptide chains. Chaos, Solitons Fractals **11**, 779–790 (2000)
16. Pang, X.F.: Improvement of the Davydov theory of bioenergy transport in protein molecular systems. Phys. Rev. E **62**, 6989–6998 (2000)
17. Merz, H., Zundel, G.: Proton conduction in bacteriorhodopsin via a hydrogen-bonded chain with large proton polarizability. Biochem. Biophys. Res. Commun. **101**, 540–546 (1981)
18. Racker, E.: A New Look at Mechanisms in Bioenergetics. Academic Press, New York (1976)
19. Förster, K., Turina, P., Drepper, F., Haehnel, W., Fischer, S., Gräber, P., Petersen, J.: Proton transport coupled ATP synthesis by the purified yeast H^+-ATP synthase in proteoliposomes. Biochim. Biophys. Acta **1797**, 1828–1837 (2010)
20. Dilley, R.A., Giaquinta, R.T.: H^+ ion transport and energy transduction in chloroplasts. Curr. Top. Membrane. Transp. **7**, 49–107 (1975)
21. Henderson, R.: The purple membrane from *Halobacterium halobium*. Annu. Rev. Biophys. Bioeng. **6**, 87–109 (1977)
22. Peyrard, M., Pnevmatikos, St., Flytzanis, N.: Dynamics of two-component solitary waves in hydrogen-bonded chains. Phys. Rev. A **36**, 903–914 (1987)
23. Gordon, A.: On soliton mechanism for diffusion of ionic defects in hydrogen-bonded solids. Nuovo Cim. **12**, 229–232 (1990)
24. Peyrard, M., Dauxois, T., Hoyet, H.: Dynamics of DNA melting. Nanobiology **1**, 313–324 (1992)
25. Hochstrasser, D., Mertens, F.G., Burrner, H.: Energy transport by lattice solitons in α-helical proteins. Phys. Rev. A **40**, 2602–2610 (1989)
26. Gaveau, B., Moreau, M., Schuman, B.: Microscopic model of the actin-myosin interaction in muscular contractions. Phys. Rev. E **69**, 011108 (2004)
27. Swanson, B., Brozik, J.A., Love, S.P., Strouse, G.F., Shreve, A.P., Bishop, A.R., Wang, W. Z. , Salkola, M.I.: Observation of intrinsically localized modes in a discrete low-dimensional material. Phys. Rev. Lett. **82**, 3288–3291 (1999)
28. Joyeux, M., Grebenshchikov, S. Yu., Bredenbeck, J., Schinke, R., Farantos, S.C.: Intramolecular dynamics along isomerization and dissociation pathways, in geometrical structures of phase space in multi-dimensional chaos. Adv. Chem. Phys. **130**, 267–303 (2005)
29. Schwarz, U.T., English, L.Q., Sievers, A.J.: Experimental generation and observation of intrinsic localized spin wave modes in an antiferromagnet. Phys. Rev. Lett. **83**, 223–226 (1999)
30. English, L.Q., Sato, M., Sievers, A.J.: Nanoscale intrinsic localized modes in an antiferromagnetic lattice. J. Appl. Phys. **89**, 6707 (2001)
31. Trias, E., Mazo, J.J., Orlando, T.P.: Discrete breathers in nonlinear lattices: experimental detection in a Josephson array. Phys. Rev. Lett. **84**, 741–744 (2000)
32. Binder, P., Abraimov, D., Ustinov, A.V., Flach, S., Zolotaryuk, Y.: Observation of breathers in Josephson ladders. Phys. Rev. Lett. **84**, 745–748 (2000)
33. Xie, A., Van der Meer, L., Hof, W., Austin, R.H.: Long-lived amide I vibrational modes in myoglobin. Phys. Rev. Lett. **84**, 5435–5438 (2000)
34. Kavitha, L., Saravanan, M., Srividya, B., Gopi, D.: Breatherlike electromagnetic wave propagation in an antiferromagnetic medium with Dzyaloshinsky–Moriya interaction. Phys. Rev. E **84**, 066608 (2011)
35. Pnevmatikos, St., Savin, A.V., Zolotaryuk, A.V., Kivshar, Yu.S., Velgakis, M.J.: Nonlinear transport in hydrogen-bonded chains: free solitonic excitations. Phys. Rev. A **43**, 5518–5536 (1991)
36. Zolotaryuk, A.V., Maniadis, P., Tsironis, G.P.: Discrete gap breathers in chains with strong hydrogen bonding. Physica B **296**, 251–258 (2001)
37. Khalack, J.M., Velgakis, M.J.: Orientational discrete breathers in hydrogen-bonded chains. Phys. Rev. E **65**, 046604 (2002)
38. Cisneros-Ake, L.A., Minzoni, A.A.: Effect of hydrogen bond anharmonicity on supersonic discrete Davydov soliton propagation. Phys. Rev. E **85**, 021925 (2012)

39. Pouthier, V.: Two-polaron energy diffusion in a one-dimensional lattice of hydrogen bounded peptide units. Physica D **237**, 106–118 (2008)
40. Pnevmatikos, St., Kivshar, Yu.S., Velgakis, M.J., Zolotaryuk, A.V.: Breathers in hydrogen-bonded chains. Phys. Lett. A **173**, 43–52 (1993)
41. Maniadis, P., Alexandrov, B.S., Bishop, A.R., Rasmussen, K.Ø.: Feigenbaum cascade of discrete breathers in a model of DNA. Phys. Rev. E **83**, 011904 (2011)
42. Hoogeboom, C., Theocharis, G., Kevrekidis, P.G.: Discrete breathers at the interface between a diatomic and a monoatomic granular chain. Phys. Rev. E **82**, 061303 (2010)
43. Ibañes, M., Sancho, J.M., Tsironis, G.P.: Dynamical properties of discrete breathers in curved chains with first and second neighbor interactions. Phys. Rev. E **65**, 041902 (2002)
44. Kavitha, L., Jayanthi, S., Muniyappan, A., Gopi, D.: Protonic transport through solitons in hydrogen-bonded systems. Phys. Scr. **84**, 035803 (2011)
45. Tokunaga, M., Matsubara, T.: Theory of ferroelectric phase transition in KH_2PO_4 type crystals. I. Prog. Theor. Phys. **35**, 581–599 (1966)
46. Holstein, T., Primakoff, H.: Field dependence of the intrinsic domain magnetization of a ferromagnet. Phys. Rev. **58**, 1098–1113 (1940)
47. Daniel, M., Kavitha, L., Amuda, R.: Soliton spin excitations in an anisotropic Heisenberg ferromagnet with octupole-dipole interaction. Phys. Rev. B **59**, 13774–13781 (1999)
48. Daniel, M., Kavitha, L.: Localized spin excitations in an anisotropic Heisenberg ferromagnet with Dzyaloshinskii–Moriya interactions. Phys. Rev. B **63**, 172302 (2001)
49. Glauber, R.J.: Coherent and incoherent states of the radiation field. Phys. Rev. **131**, 2766–2788 (1963)
50. Zakharov, V.E., Ostrovsky, L.A.: Modulation instability: the beginning. Physica D **238**, 540–548 (2009)
51. Sedletsky, Y.V.: A new type of modulation instability of Stokes waves in the framework of an extended NSE system with mean flow. J. Phys., A, Math. Gen. **39**, L529–L537 (2006)
52. Centurion, M., Porter, M.A., Pu, Y., Kevrekidis, P.G., Frantzeskakis, D.J., Psaltis, D.: Modulational instability in nonlinearity-managed optical media. Phys. Rev. A **75**, 063804 (2007)
53. Vicencio, R.A., Brand, J. Flach, S.: Fano blockade by a Bose–Einstein condensate in an optical lattice. Phys. Rev. Lett. **98**, 184102 (2007)
54. Molina, M.I., Vicencio, R.A., Kivshar, Y.S.: Two-color discrete localized modes and resonant scattering in arrays of nonlinear quadratic optical waveguides. Phys. Rev. E **72**, 036622 (2005)
55. Davydov, A.S.: Solitons in Molecular Systems. Reidel, Dordrecht (1987)
56. Dauxois, T., Peyrard, M., Bishop, A.R.: Entropy-driven DNA denaturation. Phys. Rev. E **47**, R44–R47 (1993)
57. Feldman, A.B., Chernyak, Y.B., Cohen, R.J.: Wave-front propagation in a discrete model of excitable media. Phys. Rev. E **57**, 7025–7040 (1998)
58. Bell, J.: In: Brown, K.J., Larey, A.A (eds.) Reaction–Diffusion Equations. Clarendon, Oxford (1990)
59. Ochab-Marcinek, A., Schmid, G., Goychuk, I., Hänggi, P.: Noise-assisted spike propagation in myelinated neurons. Phys. Rev. E **79**, 011904 (2009)
60. Roncaglia, R., Tsironis, G.P.: Discrete quantum motors. Phys. Rev. Lett. **81**, 10–13 (1998)
61. Ponomarev, A.V., Denisov, S., Hänggi, P.: ac-Driven atomic quantum motor. Phys. Rev. Lett. **102**, 230601 (2009)
62. Lai, R., Sievers, A.J.: Nonlinear nanoscale localization of magnetic excitations in atomic lattices. Phys. Rep. **314**, 147–236 (1999)
63. Bejot, P., Kibler, B., Hertz, E., Lavorel, B., Faucher, O.: General approach to spatiotemporal modulational instability processes. Phys. Rev. A **83**, 013830 (2011)
64. Xiang, Y., Wen, S., Dai, X., Fan, D.: Modulation instability in nonlinear oppositely directed coupler with a negative-index metamaterial channel. Phys. Rev. E **82**, 056605 (2010)
65. Tian, Q., Wu, L., Zhang, J.-F., Malomed, B.A., Mihalache, D., Liu, W.M.: Exact soliton solutions and their stability control in the nonlinear Schrödinger equation with spatiotemporally modulated nonlinearity. Phys. Rev. E **83**, 016602 (2011)
66. Misra, A.P., Shukla, P.K.: Stability and evolution of wave packets in strongly coupled degenerate plasmas. Phys. Rev. E **85**, 026409 (2012)
67. Erkintalo, M., Hammani, K., Kibler, B., Finot, C., Akhmediev, N., Dudley, J.M., Genty, G.: Higher-order modulation instability in nonlinear fiber optics. Phys. Rev. Lett. **107**, 253901 (2011)
68. Hung, N.V., Zin, P., Trippenbach, M., Malomed, B.A.: Two-dimensional solitons in media with stripe-shaped nonlinearity modulation. Phys. Rev. E **82**, 046602 (2010)
69. Assanto, G., Cisneros, L.A., Minzoni, A.A., Skuse, B.D., Smyth, N.F., Worthy, A.L.: Soliton steering by longitudinal modulation of the nonlinearity in waveguide arrays. Phys. Rev. Lett. **104**, 053903 (2010)